Basin-Scale Estimate of the Sea-Air CO2 Flux During the 2010 Warm Event in the Tropical North Atlantic

Nathalie Lefèvre, Dóris Veleda, Pedro Tyaquiçã, Coralie Perruche, Denis Diverrès, J. Severino P. Ibánhez

JGR Biogeosciences

RESEARCH ARTICLE
10.1029/2018JG004840

Basin-Scale Estimate of the Sea-Air CO_2 Flux During the 2010 Warm Event in the Tropical North Atlantic

Nathalie Lefèvre[1], Doris Veleda[2], Pedro Tyaquiçã[2], Coralie Perruche[3], Denis Diverrès[4], and J. Severino P. Ibánhez[5,6]

[1]IRD-LOCEAN, Sorbonne Université (Université Pierre et Marie Curie-CNRS-MNHN), Paris, France, [2]Department of Oceanography – DOCEAN, Federal University of Pernambuco – UFPE, Recife, PE, Brazil, [3]Mercator-Ocean, Ramonville Saint-Agne, Haute-Garonne, France, [4]US IMAGO, Centre IRD de Bretagne, Plouzané, France, [5]Biogeochemistry Research Group, School of Natural Sciences, Trinity College Dublin, College Green, Dublin, Ireland, [6]Instituto de Investigacións Mariñas, Consejo Superior de Investigaciones Científicas (IIM-CSIC), Vigo, Spain

Abstract Following the anomalous warming event occurring in the tropical North Atlantic in 2010, higher than usual surface fugacity of CO_2 (fCO_2) was observed. To evaluate the spatial extent of these anomalies and their drivers, and to quantify the sea-air CO_2 flux at basin scale, the Mercator-Ocean model is used from 2006 to 2014 within the region 0–30°N, 70–15°W. Model outputs are generally in accordance with underway sea surface temperature, sea surface salinity, and surface fCO_2 recorded by two merchant ships. The anomalous warming of 2010 is well reproduced by the model and is the main driver of fCO_2 anomalies. The first coupled Empirical Orthogonal Function mode, between sea surface temperature and fCO_2, captures more than 70% of the total variance and is characterized by a basin-scale warming associated to positive fCO_2 anomalies. The corresponding principal components are correlated to the Tropical North Atlantic Index and identify 2010 as the year with the highest positive anomaly over 2006–2014. Exceptions to this general pattern are located near the African coast, where the weakening of the coastal upwelling causes negative inorganic carbon anomalies, and close to the Amazon River plume, where fCO_2 anomalies are primarily associated with sea surface salinity anomalies. Although the fCO_2 anomalies of 2010 appear mostly in spring, they affect the annual CO_2 budget and lead to an increased CO_2 outgassing twice as large (46.2 Tg C per year) as the mean annual flux over the 2006–2014 period (23.3 Tg C per year).

Key Points:
- Underway fCO_2 observations of 2010, collected on two merchant ships, compare well with the Mercator-Ocean model simulations
- The fCO_2 anomalies observed in Spring 2010 in the tropical North Atlantic are mostly driven by the sea surface temperature anomalies
- The resulting outgassing of CO_2 for the year 2010 is twice as large as the mean sea-air CO_2 flux over the 2006 to 2014 period

Correspondence to:
N. Lefèvre,
nathalie.lefevre@locean-ipsl.upmc.fr

Citation:
Lefèvre, N., Veleda, D., Tyaquiçã, P., Perruche, C., Diverrès, D., & Ibánhez, J. S. P. (2019). Basin-scale estimate of the sea-air CO_2 flux during the 2010 warm event in the tropical North Atlantic. *Journal of Geophysical Research: Biogeosciences*, *124*, 973–986. https://doi.org/10.1029/2018JG004840

Received 27 SEP 2018
Accepted 18 MAR 2019
Accepted article online 28 MAR 2019
Published online 15 APR 2019

1. Introduction

Interannual variability in sea-air CO_2 fluxes is mainly driven by climate variability (e.g., Le Quéré et al., 2000; Park et al., 2010; Roy et al., 2011). The strongest interannual variability of the CO_2 flux occurs in the equatorial Pacific and is associated with the El Niño Southern Oscillation. During El Niño, the CO_2 outgassing of the equatorial Pacific is significantly reduced due to the weakness of the equatorial upwelling (e.g., Feely et al., 1995). Both the canonical El Niño and the El Nino-Modoki affect the sea-air CO_2 flux on interannual time scales (Valsala et al., 2014). In the North Atlantic, the role of the North Atlantic Oscillation (NAO) in the CO_2 exchange with the atmosphere has been evidenced (e.g., Levine et al., 2011; Schuster et al., 2013). Besides the NAO, one of the dominant multidecadal modes of variability in the North Atlantic is the Atlantic Multidecadal Oscillation (AMO; equator to 70°N). It represents sea surface temperature (SST) changes in the North Atlantic Ocean and is characterized by warm and cold phases as a response to the Atlantic Meridional Overturning Circulation, with a period of 60–80 years. Breeden and McKinley (2016) showed the impact of the AMO on the seawater fugacity of CO_2 (fCO_2) over the 1948–2009 period, that is a result of the direct link between the AMO and the basin-scale SST.

Most of the studies of the interannual variability of fCO_2 have focused on the equatorial Pacific due to the El Niño events, and on the North Atlantic (e.g., Loptien & Eden, 2010) as it is a strong sink of atmospheric CO_2. The tropical Atlantic has received little attention although it is the second largest source of CO_2 after the equatorial Pacific (e.g., Takahashi et al., 2014). However, current warming trend (Deser et al., 2010) is likely to increase the outgassing of CO_2 and alter the CO_2 budget in this region. In addition, Pacific-North Atlantic teleconnections may lead to strong warming events such as those observed in 2005 (Foltz & McPhaden, 2006) and 2010 in the tropical Atlantic (Taschetto et al., 2016). The impact of these events on the sea-air CO_2 flux is poorly known but the CO_2 monitoring programs provide a good means to study these events.

In the tropical Atlantic, the interannual variability is mainly governed by the Atlantic Meridional Mode (AMM), characterized by an interhemispheric SST gradient and a zonal mode similar to the El Niño in the Pacific (Brierley & Wainer, 2017). Associated to the AMM, other dominant pattern of climate variability is the Tropical North Atlantic index (TNAI) in central and eastern tropical North Atlantic, including the Cape Verde Islands (Enfield et al., 1999). TNAI exhibits interannual to multidecadal variations and is highly correlated with the AMO (Enfield et al., 2001). Also, Chen and Wu (2017) found that the springtime TNAI SST is highly correlated with the succeeding winter El Niño Southern Oscillation after the 1980s.

In 2010, the tropical North Atlantic (0–30°N) experienced anomalous surface warming conditions (Blunden et al., 2011), that resulted from a combination of mechanisms, such as the Pacific El Niño of 2009, the negative NAO and the reduced latent heat flux, and the increasing shortwave radiation (Hong et al., 2015).

Above-average SSTs were present during 2010 across the Atlantic and Indian Oceans, with the most prominent warmth across the tropical Atlantic, where the SSTA increased by 0.33 °C from 2009 to 2010 and reached a historical high (Blunden et al., 2011). Rugg et al. (2016) identified anomalous warming occurring more steadily during January–April, peaking at about 1.58 °C in April. They also argue that during the 2010 warm event, March–May meridional wind stress and thermocline depth anomalies were considerably weaker than during the same period in 2009, resulting in a much smaller contribution from these anomalies in the vertical turbulent cooling.

These conditions affected the sea-air exchange of CO_2 in this region. In the western tropical Atlantic, Lefèvre et al. (2013) observed higher-than-average salinity south of the equator in boreal spring 2010. This anomaly was explained by the anomalous position of the Intertropical Convergence Zone (ITCZ) that remained north of the equator instead of migrating south in boreal spring. The lower than usual northeastern trade winds were responsible for the anomalous northern position of the ITCZ. These conditions led to an increased CO_2 outgassing in the equatorial Atlantic in spring 2010 as observed by underway measurements made on board a Voluntary Observing Ship line from France to Brazil.

Further north, observations from two Voluntary Observing Ship lines (including the France-Brazil line explored by Lefèvre et al., 2013) also showed an anomaly of the CO_2 flux in 2010 caused by the surface warming of the ocean (Ibánhez et al., 2017). In order to provide an estimate at basin scale, Ibánhez et al. (2017), using the thermodynamic fCO_2-SST relationship of 4% per degree Celsius (Takahashi et al., 1993), calculated the expected impact of this surface warming on the CO_2 flux. The analysis of the 2010 CO_2 anomalies was thus based on observations of fCO_2 that could not cover the whole region. Furthermore, no information was collected on other parameters of the carbon cycle such as dissolved inorganic carbon (DIC) and alkalinity (TA) that could provide some insight into the actual processes responsible for the observed fCO_2 anomalies.

Here we use ocean numerical simulations to provide a complementary analysis of the basin-scale anomalies observed in 2010 in the tropical North Atlantic. First, we evaluate the performance of the model by comparing the simulations with our observations and available data fields.

Second, as the model reproduces well the 2010 warm event, we examine the impact on fCO_2 in the model and the link to climate variability. Using these model simulations, we can determine whether the temperature is the only factor explaining the fCO_2 anomalies of spring. We also identify regions where the fCO_2 anomalies are not driven by the temperature anomalies. Finally, we estimate the flux of CO_2 at basin scale in 2010 and the impact of the CO_2 anomalies on the CO_2 budget in the region over the 2006–2014 period.

2. Data and Methods

2.1. Observations and Basin-Scale Fields

During the European project CARBOOCEAN, two merchant ships were equipped with a CO_2 system to measure the fugacity of CO_2 underway using an autonomous system based on infrared detection described by Pierrot et al. (2009). The *MN Colibri*, sailing between France and French Guiana, has measured surface seawater fCO_2 since 2006. The voyages from France to Brazil, performed by the *Rio Blanco*, have started in 2008. In 2010, the *MN Colibri* realized 8 voyages along the France-French Guiana line and the *Rio*

Table 1
Voyages of the MN Colibri and the Rio Blanco in 2010

Reference	Dates of the voyages	Vessel name	Minimum latitude (°N)	Maximum latitude (°N)	Route
RB1	18–22 January 2010	Rio Blanco	0	30	France-Brazil
RB2	10–14 February 2010	Rio Blanco	0	30	Brazil-France
RB3	1–5 March 2010	Rio Blanco	0	30	France-Brazil
RB4	24–28 March 2010	Rio Blanco	0	30	Brazil-France
C1	1–5 April 2010	Colibri	6.7	30	France-French Guiana
C2	11–17 April 2010	Colibri	8	30	French Guiana-France
RB5	10–15 May 2010	Rio Blanco	0	30	Brazil-France
C3	18–24 May 2010	Colibri	5.7	30	France-French Guiana
RB6	1–6 June 2010	Rio Blanco	0	30	France-Brazil
C4	20–26 June 2010	Colibri	8.5	30	French Guiana-France
RB7	28 June to 3 July 2010	Rio Blanco	0	30	Brazil-France
RB8	20–25 July 2010	Rio Blanco	0	30	France-Brazil
C5	3–8 August 2010	Colibri	7	30	France-French Guiana
C6	15–18 August 2010	Colibri	14.8	30	French Guiana-France
RB9	16–21 August 2010	Rio Blanco	0	30	Brazil-France
RB10	7–12 September 2010	Rio Blanco	0	30	France-Brazil
RB11	5–9 October 2010	Rio Blanco	0	30	Brazil-France
C7	6–10 October 2010	Colibri	11	30	France-French Guiana
C8	18–22 October 2010	Colibri	10	25.6	French Guiana-France
RB12	26–30 October 2010	Rio Blanco	0	30	France-Brazil
RB13	22–27 November 2010	Rio Blanco	0	30	Brazil-France

Blanco realized 13 voyages along the France-Brazil line (Table 1). The fCO_2 data corresponding to these two commercial lines are available in the SOCAT database (www.socat.info, Bakker et al., 2016).

In addition to the data collected along the tracks of the ships, we used observations available at the basin scale. Monthly SST fields were obtained from the daily NOAA Optimum Interpolation SST v2 data on a 0.25° resolution (Reynolds et al., 2007). Monthly sea surface salinity (SSS) fields were obtained from the Soil Moisture and Ocean Salinity (SMOS) mission at IFREMER (https://www.catds.fr). SMOS data version 2 are available from May to December 2010. The data acquired during the first 4 months of the commissioning phase in 2010 were not reprocessed because of reduced data quality during that period just post launch. However, data from January to April 2010 are available in version 1 and are used to complete the comparison of SSS with the model outputs during this period.

The monthly Era-Interim wind field at 10 m was used and downloaded from the European Centre for Medium-Range Weather Forecasts at a resolution of 0.25° and available at http://www.ecmwf.int/ (Dee et al., 2011).

2.2. Model Simulations

The Mercator-Ocean simulation is based on the NEMO modeling platform (Nucleus for European Modeling of the Ocean) and covers the global ocean with a spatial resolution of 0.25° over the 1997–2014 period. The biogeochemical NEMO component PISCES (NEMO version 3.5) is coupled offline to the hydrodynamic NEMO component OPA (NEMO version 3.1) at a daily frequency. The biogeochemical simulation (product 001_018) is available on request on the Mercator-Ocean portal (https://www.mercator-ocean.fr/en). The detailed features of this simulation are described in the Quality Information Document (http://marine.copernicus.eu/documents/QUID/CMEMS-GLO-QUID-001-018.pdf). Biogeochemical and physical simulations start at rest in December 1991 with the Levitus climatology of 1998 for temperature and salinity; the World Ocean Atlas 2001 for nitrate, phosphate, oxygen, and silicate (Conkright et al., 2002); and the GLODAPv1 for alkalinity and DIC (Key et al., 2005) as initial conditions. Nutrients are supplied to the ocean via three different external sources (Aumont et al., 2015): atmospheric deposition of Fe, Si, and P; river supply of N, P, Fe, Si, and C; and inputs of Fe from marine sediments. River supplies of biogeochemical parameters are collocated with freshwater inflows prescribed by the physical model. A monthly runoff climatology is used to force the hydrodynamic model. It is built with data of coastal runoffs from 100 major rivers (Dai & Trenberth, 2002). River nutrient discharge is provided by a monthly climatology based on the

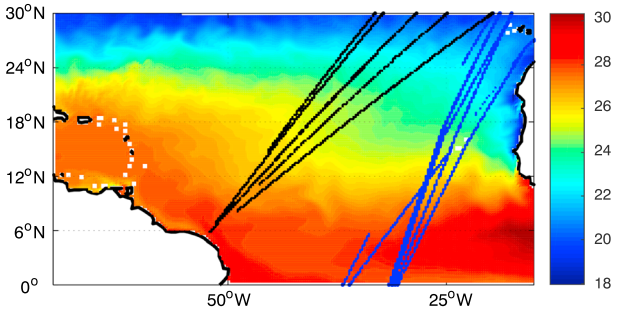

Figure 1. Map of modeled sea surface temperature in March 2010 with the tracks of the France-French Guiana line (in black) and the France-Brazil line (in blue) for the year 2010.

model GLOBAL-NEWS2 (Mayorga et al., 2010) and the Global Erosion Model of Ludwig et al. (1996). The PISCES model simulates the biogeochemical cycles of oxygen, carbon, and major nutrients controlling phytoplankton growth (P, N, Fe, and Si). Among other variables, PISCES simulates DIC and TA (Aumont et al., 2015; Aumont & Bopp, 2006). The CO_2 chemistry is computed following the OCMIP protocols (http://www.ipsl.jussieu.fr/OCMIP). We extracted the region bounded by 0–30°N and 70–15°W. Figure 1 shows the domain of study with the tracks of the voyages superimposed on the modeled SST of March 2010.

The model outputs used here are daily means of temperature, salinity, DIC, and TA. Using these parameters for the surface layer of the ocean, we calculated seawater fCO_2 (fCO_{2sw}) applying the dissociation constants of Mehrbach et al. (1973) refitted by Dickson and Millero (1987) and the CO2SYS program for Matlab. This fCO_{2sw} value is referred to as the Mercator or modeled fCO_{2sw} hereafter.

The sea-air flux of CO_2 is then calculated as follows:

$$F = k\,S\,(fCO_{2sw} - fCO_{2atm}), \quad (1)$$

where k is the gas exchange coefficient from Sweeney et al. (2007), S is the solubility of CO_2 in seawater (Weiss, 1974), and fCO_{2atm} is the atmospheric fCO_2. fCO_{2atm} is calculated from the interpolated molar fraction of CO_2 at different atmospheric stations of the NOAA network as described by Ibánhez et al. (2017). For the calculation of k, we used the wind speed at 10 m, available from ERA-Interim reanalysis (European Centre for Medium-Range Weather Forecasts). A positive flux indicates a source of CO_2 to the atmosphere.

2.3. Model Validation and Performance

The 21 voyages performed by the voluntary ships used here during 2010 (Table 1) were used to evaluate the performance of the Mercator-Ocean model in the tropical Atlantic. The modeled values of temperature, salinity, DIC, and TA were extracted along the track of each voyage for the time period spanning the 0–30°N latitudinal range (Table 1). The calculated fCO_{2sw} from modeled DIC and TA were then compared to the fCO_{2sw} observations obtained along the tracks of the ships.

A Taylor diagram (Taylor, 2001) was used to compare the model results and the observations. This diagram provides a graphical representation of how closely a simulation matches the observations. The correlation coefficient, the standard deviation, and the centered root-mean-square difference are the three statistical parameters displayed on the diagram.

2.4. Statistical Analysis

In order to study the link between the observed anomalies and climate variability, we performed a coupled empirical orthogonal function (EOF) analysis applied to the daily SST from 2006 to 2014 and the fCO_2 calculated using DIC and TA extracted from the Mercator-Ocean model. The daily climatologies of SST and fCO_2 were removed before the analysis. To explain the interannual variability, the principal components (PCs) of each EOF mode are monthly averaged and correlated with predominant climatic indices in the region.

3. Results and Discussion

3.1. Comparison Between Model Outputs and Observations for the Year 2010

The model outputs corresponding to the year 2010 are compared with observations made along the tracks of the merchant ships and with basin-scale fields. The voyages of the *Rio Blanco* in July 2010 and of the *MN Colibri* in August 2010 are presented with the collocated model outputs along the tracks, as an example of the comparison of the model results with the 21 voyages (Figure 2). Similar agreement is found for the other transects. The modeled SST is in very good agreement with the underway observations (Figures 2a and 2b) but slightly lower along the France-French Guiana line. The model reproduces well the salinity distribution

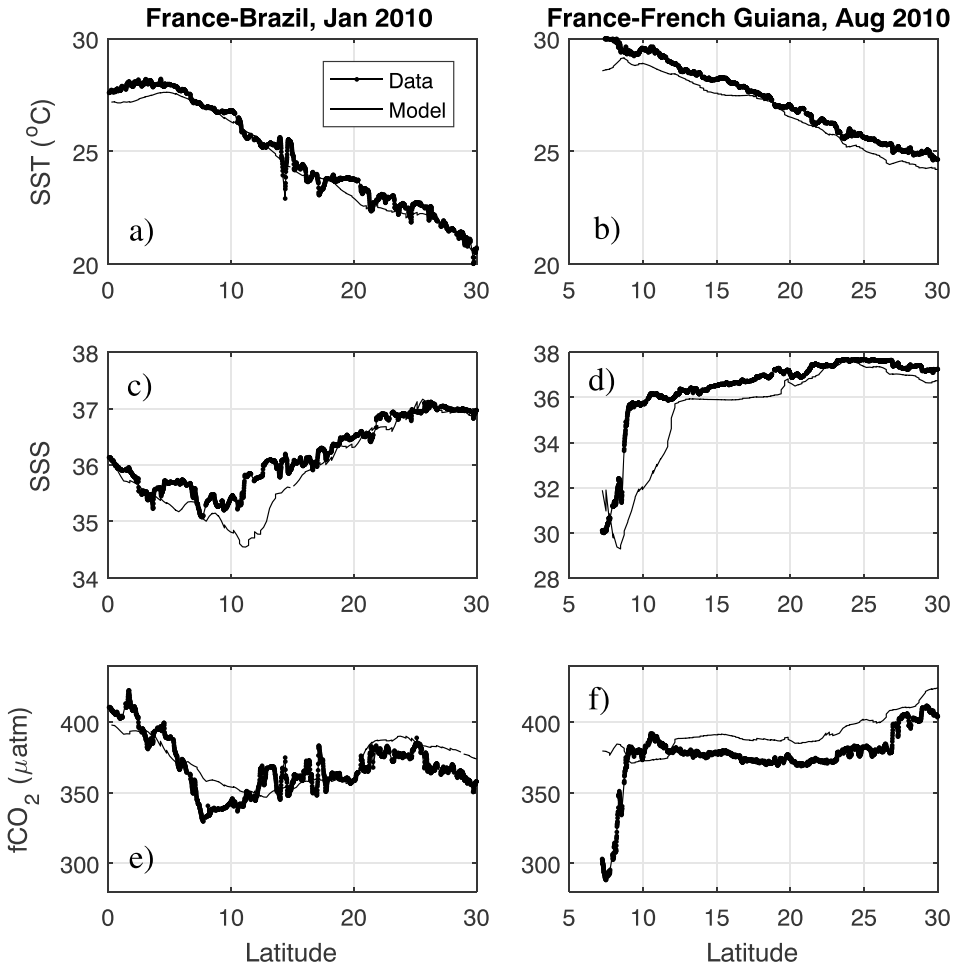

Figure 2. Latitudinal distributions of (a and b) SST, (c and d) SSS, and (e and f) fCO_2 along the track of the France-Brazil line in January 2010 and the France-French Guiana line in August 2010. SST = sea surface temperature; SSS = sea surface salinity; fCO_2 = fugacity of CO_2.

but tends to be fresher (Figures 2c and 2d). The highest discrepancy occurs near the Kourou region (5–10°N) along the France-French Guiana line where the influence of the Amazon outflow is strong (Figure 2d). Along the France-Brazil line, the fCO_2 distribution is well reproduced by the model (Figure 2e). Near the Amazon outflow, the model does not reproduce the decrease of fCO_2 associated with the Amazon plume, although the modeled SSS shows a large decrease (Figure 2d) and the modeled fCO_2 remains at high oceanic levels (Figure 2f).

The results of the comparison of the Mercator-Ocean model with the France-Brazil line are summarized in a Taylor diagram (Figure 3) and each cruise is identified with its reference label given in Table 1. The correlation between modeled and observed SST is always between 0.97 and 0.99 with a root-mean-square difference between 0.2 and 0.6 °C and a standard deviation similar to the observed variations of SST (Figure 3a). The modeled SSS is usually well reproduced by the Mercator-Ocean model but exhibits higher variability than the observations (Figure 3b). The performance of the modeled fCO_2 shows high variability between the voyages. The highest discrepancy is observed in July 2010 and is explained by modeled fCO_2 higher than the observations by about 20 μatm in the 20–30°N latitudinal band (Figure 2e).

The Taylor diagram along the France-French Guiana line is shown in Figure 4. As for the France-Brazil line, the SST is well reproduced by the model (Figure 4a). Regarding the salinity, the model is not as good as along the France-Brazil line. The correlation coefficient is still higher than 0.7 and the model results show more variability than the observations except for one voyage in early October 2010 (Figure 4b).

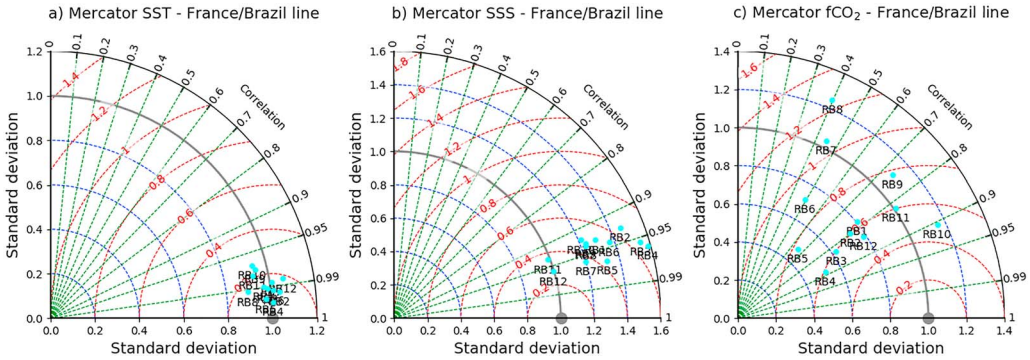

Figure 3. Taylor diagram for modeled (a) SST, (b) SSS, and (c) fCO_2 compared to the voyages along the France-Brazil line. The root-mean-square difference and the standard deviations are normalized and nondimensional as they were divided by the standard deviation of the observations to include all the voyages on the same diagram. The reference is indicated in gray. SST = sea surface temperature; SSS = sea surface salinity; fCO_2 = fugacity of CO_2.

As illustrated in Figures 2d and 2f, the region close to the Amazon outflow is the main region of discrepancy between the model and the observed SSS, which explains the difficulty to simulate fCO_2 correctly in this region. The western tropical Atlantic is characterized by numerous rings (e.g., Fratantoni & Glickson, 2001) and the spreading of the Amazon plume, which promotes a large spatial and temporal variability of these parameters even at the scale of days (Ibánhez et al., 2015). In addition, the Mercator-Ocean model uses climatological monthly river discharge data to simulate the impact of rivers into the ocean. In 2010, the Amazon river showed a pronounced negative discharge anomaly which affected both the extension and the atmospheric CO_2 drawdown associated to the river plume (Ibánhez et al., 2016). These characteristics are not appropriately simulated by the Mercator-Ocean model and thus large differences between simulated and observed salinity (and fCO_2) are expected in the region of the Amazon plume. In fact, the root-mean-square difference between these two salinity fields reach values higher than 2 psu in the vicinity of the Amazon mouth. The differences between the modeled and the observed salinities impact the distribution of fCO_2. May–June is the period of highest discharge of the Amazon and corresponds to the highest fCO_2 differences between the model and the observations as shown by the very low correlation coefficients (Figure 4c). However, after removing the data where root-mean-square difference >1.5, the fCO_2 results at the basin scale remain unchanged, which suggests that the discrepancy has a local impact only. Therefore, the area of the Amazon plume was not removed when performing basin-wide calculations.

In addition to observations along the tracks of the merchant ships, we also compared the modeled SST and SSS with basin-scale fields obtained from Reynolds Optimum Interpolation v2 (January to December 2010) and from SMOS (January to April, V1 and May to December 2010, V2), respectively (Figure 5). All the data of each month of 2010 are compared with the corresponding observations in the region 0–30°N, 70–15°W. The

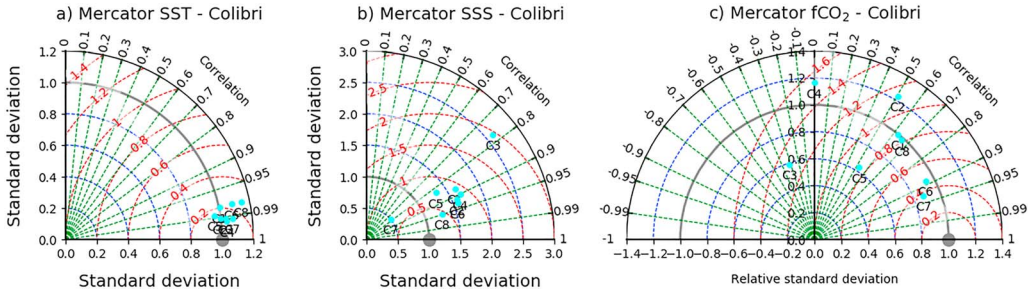

Figure 4. Taylor diagram for modeled (a) SST, (b) SSS, and (c) fCO_2 compared to the voyages along the France-French Guiana line. The root-mean-square difference and the standard deviations are normalized and nondimensional as they were divided by the standard deviation of the observations to include all the voyages on the same diagram. The reference is indicated in gray. SST = sea surface temperature; SSS = sea surface salinity; fCO_2 = fugacity of CO_2.

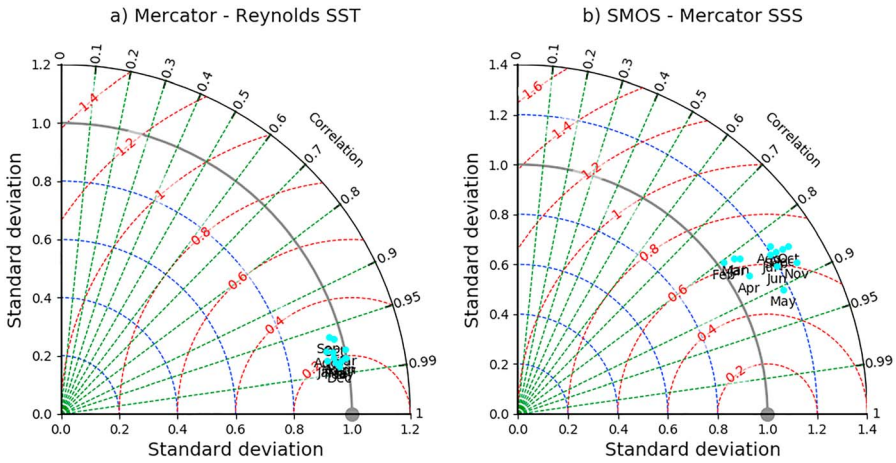

Figure 5. Taylor diagram for monthly (a) Mercator-Ocean and Reynolds SST and (b) Mercator-Ocean and SMOS SSS in 2010. SST = sea surface temperature; SMOS = Soil Moisture and Ocean Salinity; SSS = sea surface salinity.

main conclusions of the comparison along the tracks of the ships remain valid at basin scale. The temperature field is well simulated by the model with a correlation coefficient higher than 0.95 (Figure 5a). The comparison of SSS along the tracks of the ships presents some discrepancy mainly in the North Brazil Current and Amazon outflow region. At the basin scale, the comparison with the SSS from SMOS for each month of 2010 in the region 0–30°N, 70–15°W gives a correlation coefficient higher than 0.8 with a standard deviation higher than the one given by the observations. A similar result is obtained along the tracks of the ships except for a few voyages. Overall, the measurements taken on board the merchant ships give similar statistics as the comparison between the basin SST and SSS fields and the model results.

3.2. Basin-Scale Anomalies in the Tropical North Atlantic During 2010

The Mercator-Ocean model reproduces well the 2010 warm event. The comparison of the monthly SSTA of 2010 between the model and the Reynolds data shows a correlation coefficient ranging from 0.77 to 0.93 (Figure 6).

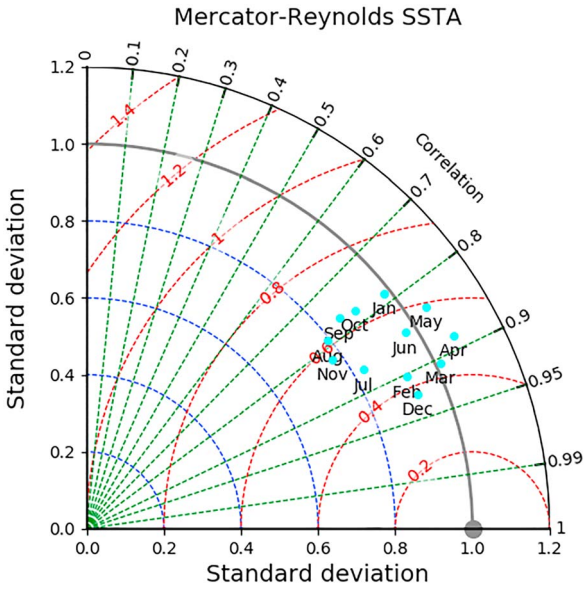

Figure 6. Taylor diagram for monthly Mercator-Ocean and Reynolds SSTA of 2010. SSTA = sea surface temperature anomaly.

As observed by Ibánhez et al. (2017), the strongest positive SSTA occur mainly in February–May 2010. The strongest SSTA are observed close to the African coast and spread westward. There, SSTA are sometimes higher than 2.5 °C. Throughout the basin, SSTA >1 °C are encountered from the eastern to the western coast in spring 2010. In the western tropical Atlantic, near the American coast, the SSTA are mainly present south of 20°N. From June 2010, the warming of the basin is decreasing, but remains strong near the African coast. In December 2010, a strong positive SSTA is observed in the region of the coastal upwelling of Mauritania. In contrast, negative SSTA are almost throughout the year 2010 observed in the north westernmost region of the basin. Thus, the warming occurs mainly in the equatorial region and in the southern part of the subtropical gyre.

Current atmospheric CO_2 increase leads to a seawater fCO_2 increase. Different studies in the tropical region reported an increase of seawater fCO_2 slightly lower than the atmospheric CO_2 increase (e.g., Lefèvre et al., 2014; Park & Wanninkhof, 2012). Using an annual seawater fCO_2 increase of 1.1 μatm/year (Park & Wanninkhof, 2012), we use the results of the Mercator model to build a climatology of seawater fCO_2 over the 2006–2014 period, referenced to the year 2010 as in Ibánhez et al. (2017). The seawater fCO_2 anomalies (fCO_2A) of 2010 are the difference between the 2010 fCO_2 and this climatology. The maps of fCO_2A exhibit

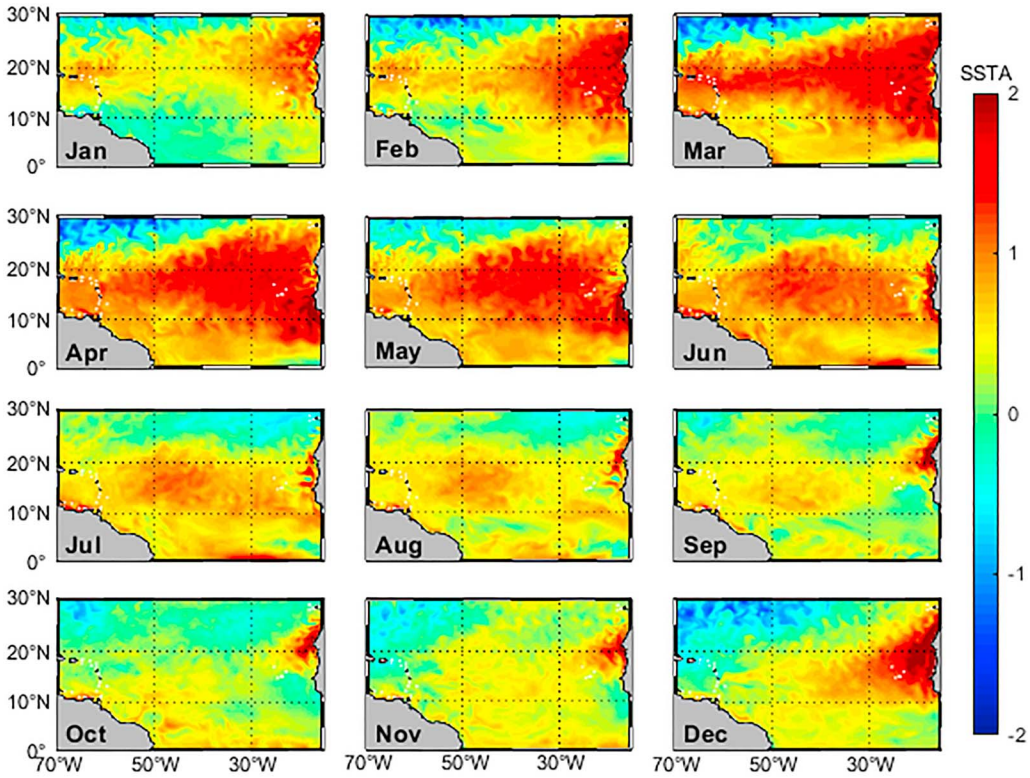

Figure 7. Monthly maps of modeled SSTA (in °C), calculated over the 2006–2014 period, for the year 2010. SSTA = sea surface temperature anomaly.

the highest values during the first half of the year (Figure 8, January to June). In March and April 2010, the positive fCO_2A correspond to the positive SSTA except near the African coast where negative fCO_2A are observed. From July 2010, positive SSTA are still present but weaker compared to those observed during the previous months. Accordingly, during the second half of the year, the strong positive fCO_2A observed during boreal spring have vanished and seawater fCO_2 become closer to the climatological values (Figure 8, July to December). In December 2010, offshore the African coast, a large area exhibits SSTA higher than 1 °C (Figure 7) associated with positive fCO_2A (Figure 8) suggesting a predominant warming effect.

The monthly maps of SSS anomalies (SSSA), DIC anomalies (DICA), and TA anomalies do not exhibit significant patterns (not shown) unlike the maps of SSTA and fCO_2A.

On average for the tropical North Atlantic, SSTA and fCO_2A are visible during spring 2010 (Figures 9a and 9b). From January to May 2010, mean DIC and TA anomalies are less than 5 μmol/kg (Figure 9c). The wind speed is lower than the climatological mean during that period (Figure 9d). This is consistent with the weaker northeast trade winds and the anomalous position of the ITCZ reported by Lefèvre et al. (2013). When compared to the monthly wind speed climatology from 2006 to 2014, the wind speed in 2010 is lower than the climatology (t test, p-value = 0.006), whereas the other years have a similar mean as the climatology. From July to December 2010, positive SSTA remain but are much lower (Figure 9a). The slightly negative fCO_2A are associated with negative DICA (Figures 9b and 9c). At basin scale, fCO_2A are mainly caused by positive SSTA and occur during the first half of the year 2010.

3.3. Localized Anomalies During 2010

The mean anomalies at basin scale highlight the strong SSTA and fCO_2A co-occurrence during the spring 2010 and are mainly located between the equator and 20°N (Figures 7 and 8). Nevertheless, DICA do not follow the general SSTA or fCO_2A patterns and are negative from April to December 2010 on average in the whole region (not shown). In the African upwelling, positive SSTA (Figure 10a) are associated with

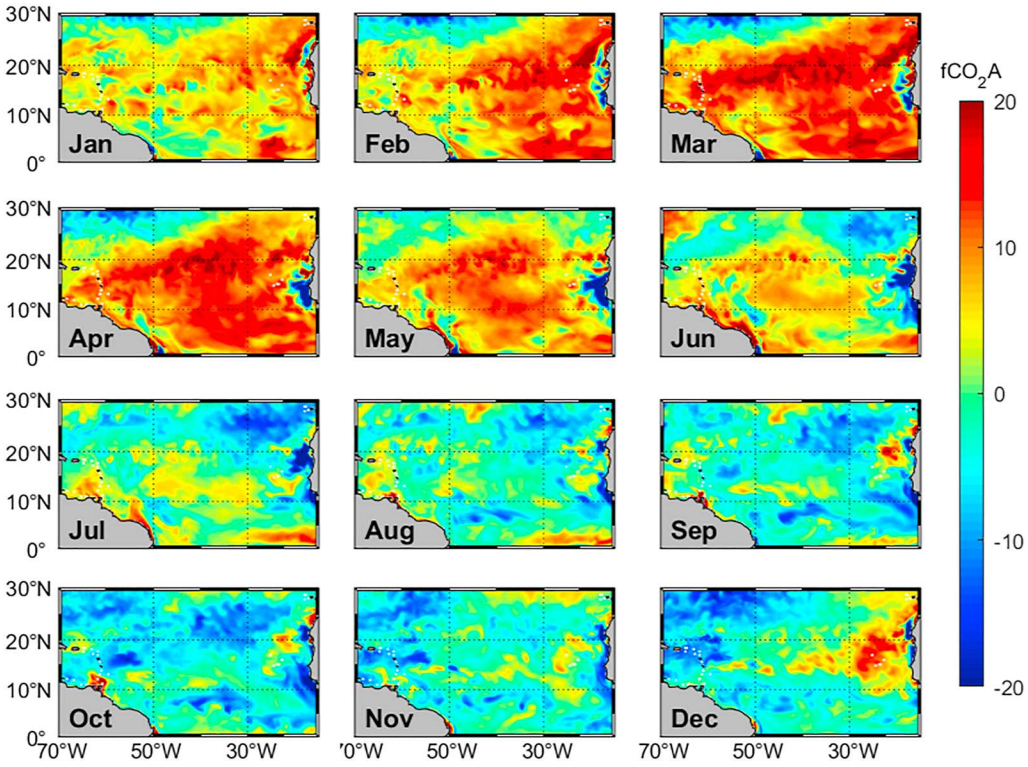

Figure 8. Monthly maps of fCO_2A (in μatm) from January to December 2010 calculated over the 2006–2014 period. fCO_2A = fugacity of CO_2 anomaly.

strong negative DICA (Figure 10b), concomitant with negative fCO_2A (Figure 10c). These negative fCO_2A are especially striking from March to May 2010 when SSTA are the strongest (Figure 8). The strong positive SSTA from 10 to 16°N (Figure 10a) suggest a reduced upwelling. The upwelling brings cold waters with high CO_2 content to the surface, the deeper the water the richer the CO_2 content. In case of reduced upwelling, the water comes from shallower depth and the CO_2 content is poorer. This leads to lower-than-usual surface fCO_2, hence the negative fCO_2A (Figure 9c). These negative fCO_2A close to the African coast appear during all the months of 2010 (Figure 8). The spatial correlation between DICA and fCO_2A is always above 0.64 and is stronger from February to June 2010 with a coefficient above 0.83 in the 10–22°N, 15–20°W region. Furthermore, these appear negatively correlated with SSTA in the region. As an example, in April 2010, within the 10–22°N, 15–20°W region, fCO_2A and DICA are negatively correlated with SSTA (−0.72 and −0.87, respectively) and the correlation between fCO_2A and DICA is positive (0.90).

Negative fCO_2A are mainly present south of 16°N. North of 16°N, these negative anomalies vanish. Menna et al. (2016) show a different behavior of the upwelling off the coast of north-western Africa. They find that the southern sector south of 16°N has most favorable upwelling conditions in December–June and strongly depends on the wind forcing. They report that the northern sector does not show significant correlation with the wind stress. In 2010, the weakening of the northeastern trade winds may have affected mostly the southern sector causing the reduced upwelling and the negative DICA showed by the model results.

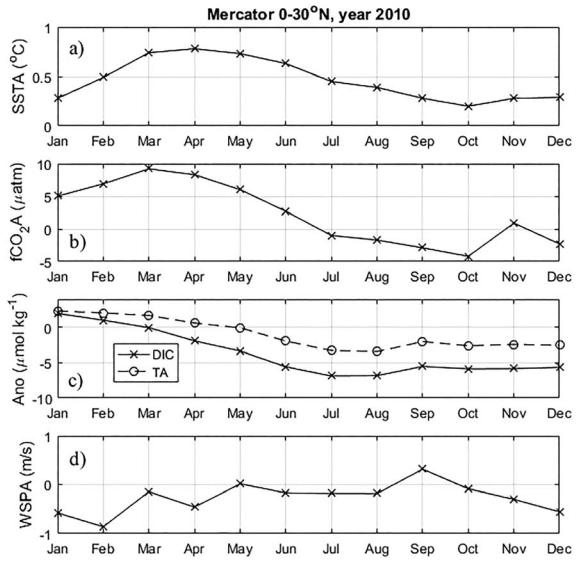

Figure 9. Basin-scale anomalies of (a) SST, (b) seawater fCO_2, (c) DIC and TA, and (d) wind speed at 10 m in 2010. fCO_2A = fugacity of CO_2 anomaly; SSTA = sea surface temperature anomaly; DIC = dissolved inorganic carbon; TA = alkalinity.

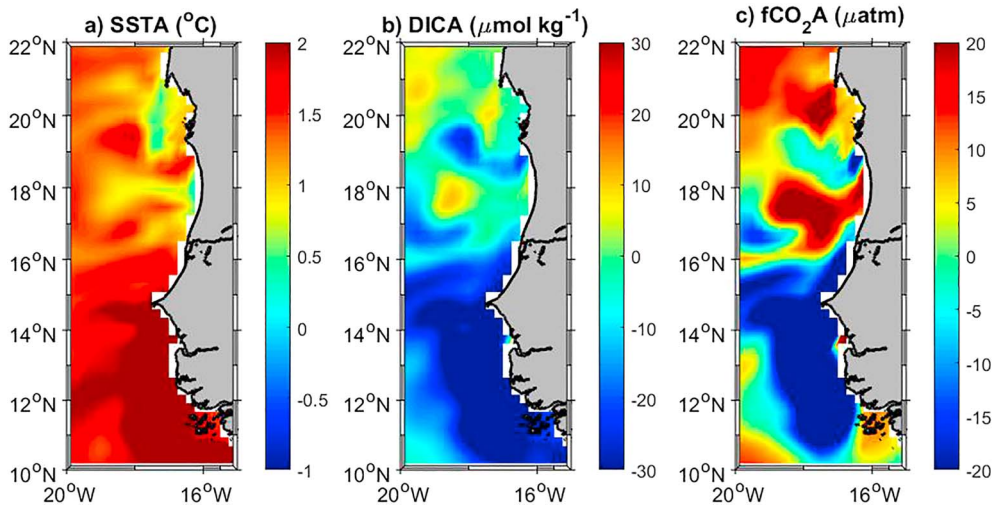

Figure 10. (a) SSTA, (b) DICA, and (c) fCO_2A close to the coast of Africa in April 2010. SSTA = sea surface temperature anomaly; DICA = dissolved inorganic carbon anomalies; fCO_2A = fugacity of CO_2 anomaly.

During the highest Amazon discharge, in May–June, positive anomalies of SSS occur close to the Amazon mouth, near the equator, in 2010 (not shown). However, these SSSA are probably underestimated because, as previously discussed, the model is forced with a monthly climatology of river discharge and thus does not reproduce the negative discharge anomalies observed in 2010 (Ibánhez et al., 2016). The retroflection of the North Brazil Current starts in July and transports Amazon waters eastward in the North Equatorial Counter Current. In the region including the Amazon plume and part of the North Equatorial Counter Current (0–12°N, 60–40°W), fCO_2A associated with SSTA occur mainly during the first months of 2010 (Figures 11a and 11b). Although SSTA remain positive in the second part of the year, the negative DICA are the main driver of the fCO_2A that become negative. DICA are strongly correlated with the SSSA ($r > 0.99$). Negative DICA start at the time of the highest Amazon discharge and remain until the end of 2010. Positive SSTA and negative DICA act in opposite way on fCO_2. The warming tends to increase fCO_2 whereas the decrease of DIC reduces fCO_2. Thus, the slight negative fCO_2A observed from August to December 2010 in this region suggest that fCO_2A are mainly controlled by DICA ($r = 0.65$), and hence SSSA, rather than by SSTA ($r = 0.46$) in the region of the Amazon plume.

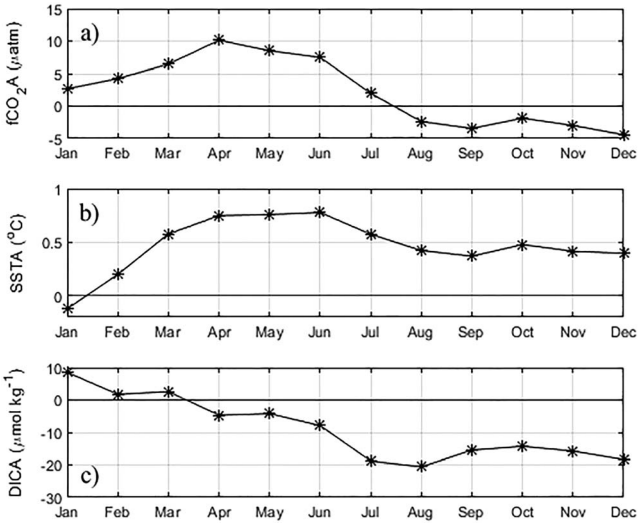

Figure 11. Time-series of monthly anomalies of (a) fCO_2, (b) SST, and (c) DIC in the region of the Amazon plume and NECC (0–12°N, 60–40°W) in 2010. DICA = dissolved inorganic carbon anomalies; SSTA = sea surface temperature anomaly; fCO_2A = fugacity of CO_2 anomaly.

3.4. Origin of the 2010 SST Anomalies

The strong co-occurrence of SSTA and fCO_2A observed suggest that the warming of the basin is the dominant process responsible for the unusual seawater fCO_2 increase in the first half of 2010. A coupled EOF is performed to identify the dominant modes of variability in the 0–30°N region and to better understand the 2010 warming anomaly.

The first two EOF modes together explain 86.8% of the total covariance between SST and fCO_2, with each mode containing 70.3% and 16.5% of the total covariance, respectively.

In the first EOF mode, the spatial pattern of SST is characterized by a basin-scale warming from the central to the eastern North Atlantic, associated with positive fCO_2 anomalies (Figures 12a and 12b). Associated to the first mode in SST, fCO_2 also presents a positive anomaly pattern in the central and eastern North Atlantic, except in the upwelling region confined along the African coast, where the fCO_2 anomalies are negative and, to a lesser extent, the region of the Amazon plume where fCO_2A are more related to SSSA as discussed before. This first mode of fCO_2 is similar to the fCO_2 anomalies identified in 2010 (Ibánhez et al., 2017). The PC

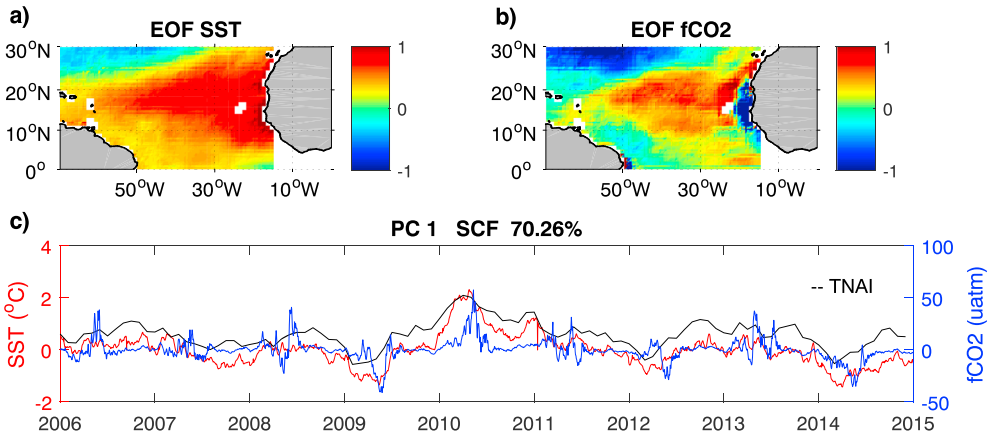

Figure 12. (a) First EOF of SST, (b) first EOF of fCO_2, and (c) first PC of the coupled EOF between SST and fCO_2. EOF = empirical orthogonal function; SST = sea surface temperature; fCO_2 = fugacity of CO_2; PC = principal component; SCF = Squared Covariance Fraction.

associated to the first mode of both parameters (Figure 12c) displays a coupled time evolution, evidencing the strongest positive SST anomaly in 2010. This coupled pattern confirms an interannual dependence of the fCO_2 on the SST variability in the western tropical Atlantic. The PCs of both variables were monthly averaged to correlate with the climatic indices. At zero lag, the first PC (PC1) of SST has a correlation of 0.92 with TNAI, 0.72 with AMM, and 0.61 with AMO. The PC1 of fCO_2 is correlated with TNAI (0.6), AMM (0.52), and AMO (0.42). TNAI and AMO present a strong positive phase during the year of 2010, associated with the observed sea surface warming (Figure 12). The TNAI (Enfield et al., 1999) is a climatic index calculated over the tropical North Atlantic region, covering the easternmost portion close to the

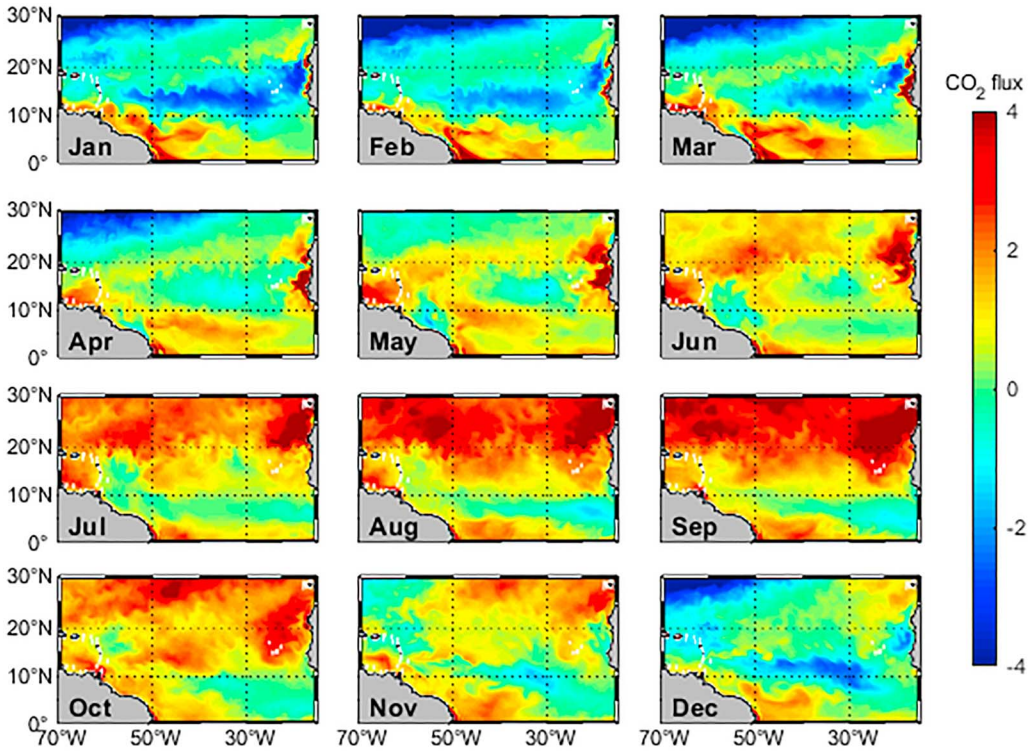

Figure 13. Monthly maps of the sea-air CO_2 flux (in $mmol \cdot m^{-2} \cdot day^{-1}$) from January to December 2010 (positive flux means outgassing of CO_2).

Table 2
Annual Wind Speed at 10 m (m/s), Wind Speed Anomaly (m/s), and CO_2 Flux (in mmol·m^{-2}·day^{-1}) From 2006 to 2014 in the Region 0–30°N, 70–15°W

Year	Wind speed	Wind speed anomaly	CO_2 flux Mercator-Ocean
2006	6.03	0.00	0.45
2007	6.07	0.03	0.40
2008	5.98	−0.05	0.44
2009	6.18	0.15	0.38
2010	5.76	−0.28	0.62
2011	6.05	0.02	−0.07
2012	5.99	−0.05	0.16
2013	6.07	0.04	0.19
2014	6.18	0.14	0.31

African coast. As the TNAI covers better the region of study, it captures better the main interannual variability of SST and consequently of fCO_2. Over the period 2006–2014, the correlation between AMO and TNAI is 0.73. Breeden and McKinley (2016) show that positive AMO leads to an increase of fCO_2 in the subtropical gyre due to the increase of SST. As the region 0–30°N includes part of the subtropical gyre, the PC1 of SST and fCO_2 is correlated with the AMO but correlations are stronger with the TNAI. The spatial pattern of the second EOF coupled mode (not shown) is characterized by negative SSTA in the eastern basin north of 20°N, and a warm area, restricted from the equator to 20°N. This mode represents about 16% of the covariance between SST and fCO_2. However, the spatial pattern of this PC is not associated to the fCO_2 variability during the period of study.

3.5. Basin-Scale CO_2 Flux in 2010

The CO_2 flux in the tropical North Atlantic is calculated from the seawater fCO_2 obtained from the Mercator-Ocean simulation, the monthly atmospheric fCO_2, and the Era-Interim wind speed at 10 m (Figure 13). The monthly CO_2 flux in 2010 is lower in winter and higher in summer as it follows the seasonal cycle of SST in the region. Even with higher seawater fCO_2 than usual in spring 2010, the seasonal pattern remains, and the CO_2 flux is still higher during summer.

From January to May 2010, the wind speed is weaker especially from January to April where the wind anomaly ranges from −0.86 to −0.14 m/s (Figure 9d). As the wind intensity is significantly weaker in 2010, the absorption of CO_2 is strongly reduced during this part of the year compared to other years. After a period of weak wind anomalies, a strong decrease of the wind intensity occurs again in November–December 2010 with a wind anomaly of −0.43 m/s. On annual average, 2010 is characterized by a lower wind speed than the other years from 2006 to 2014 (Table 2).

As the lower wind intensity occurred mainly in winter 2010, the fCO_2 anomaly associated to the strong warming in spring 2010 leads to a significant reduction of the atmospheric CO_2 absorption from January to May 2010 at the basin scale (Figure 14). The climatological sink of CO_2 observed in the tropical North Atlantic during the first months of the year has even reversed to a source in 2010. This fact corroborates with Ibánhez et al. (2017), that have identified an abrupt change of CO_2 sink of −29.3 Tg C to a source of CO_2 to the atmosphere of 1.6 Tg C from February to May of 2010. The Mercator-Ocean model gives a source of 0.01 mmol·m^{-2}·day^{-1} from February to May 2010 (which corresponds to 0.24 Tg C), whereas the same period averaged over 2006–2014 is a sink of CO_2 of −0.89 mmol·m^{-2}·day^{-1} (−22 Tg C). From June to December 2010, the CO_2 flux is similar to the flux observed during the other years analyzed here. On annual average, the CO_2 flux in the tropical North Atlantic in 2010 is 0.62 mmol·m^{-2}·day^{-1}, which gives a CO_2 outgassing of 46.2 Tg C per year for the region. The mean annual flux in the northern tropical Atlantic over the 2006–2014 period is 0.31 mmol·m^{-2}·day^{-1}, which gives an outgassing of 23.3 Tg C per year, half the value of 2010.

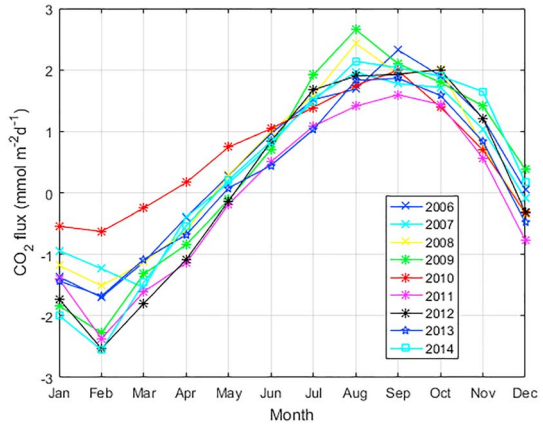

Figure 14. Monthly means of the CO_2 flux (in mmol·m^{-2}·day^{-1}) from 2006 to 2014.

4. Conclusions

Following the anomalous warming event occurring in the tropical North Atlantic in 2010, simulations of the Mercator-ocean model have been used to quantify the CO_2 flux in 2010 at basin scale and to determine the drivers of the 2010 fCO_2 anomalies.

SST, SSS, and fCO_2 observations of 2010 from two merchant ships are generally in good agreement with the collocated Mercator-Ocean model outputs. The largest differences among Mercator-Ocean results and underway measurements are encountered in the western tropical Atlantic near the Amazon outflow region. The ocean dynamics is particularly complex with the numerous rings that develop in this area. In

addition, the model is forced by a climatology of river discharge and, hence, does not consider the lower discharge of the Amazon river observed in 2010. The monthly salinity outputs are in agreement with the SMOS salinity fields but also exhibit the largest differences in this region.

SST fields and SSTA of 2010 are well reproduced by the model. Over the 2006–2014 period, the strongest positive fCO_2 anomalies occur in boreal spring 2010, when the SST anomalies are the highest. At the basin scale, the fCO_2A are not associated with anomalies of DIC and TA, which confirms that SSTA is the main driver of the fCO_2A. However, near the African coast, strong positive SSTA associated with strong negative DICA and fCO_2A are explained by a weakening of the coastal upwelling in 2010, probably caused by the weaker northeastern trade winds. Near the Amazon plume region, fCO_2A are primarily controlled by DICA that follow closely SSSA. Overall, the fCO_2A of 2010 affect the CO_2 budget of the tropical North Atlantic and lead to an increased CO_2 outgassing twice as large (46.2 Tg C per year) as the climatological mean over the 2006–2014 period of 23.3 Tg C per year.

SSTA are attributed to a combination of climatic events, evidenced through the strong positive TNAI and AMO in 2010, that affected the tropical North Atlantic and the surface fCO_2. The first PC of SSTA and fCO_2A presents the strongest positive anomaly in 2010, which is a response to the TNAI. This analysis suggests that low-frequency modes as TNA index lead to SST anomalies that affect biogeochemical processes. Thus, this index could help to monitor the sea-air CO_2 exchange in the tropical North Atlantic at interannual time scales.

Acknowledgments
The CO_2 observations have been funded and maintained by the European Integrated Projects CARBOCHANGE (grant agreement 264879), AtlantOS (grant agreement 633211), ICOS France Océan, and the Institut de Recherche pour le Développement (IRD). The fCO_2 data are available in the SOCAT database (http://www.socat.info). Sea surface salinity data derived from thermosalinograph instruments installed onboard the *MN Colibri* and the *Rio Blanco* were collected, validated, archived, and made freely available by the French Sea Surface Salinity Observation Service (http://www.legos.obs-mip.fr/observations/sss/). NOAA High Resolution SST data are provided by the NOAA/OAR/ESRL PSD, Boulder, Colorado, USA, from their website (at https://www.esrl.noaa.gov/psd/). The SMOS SSS data were obtained from the Ocean Salinity Expertise Center (CECOS) of the CNES-IFREMER Centre Aval de Traitement des Données SMOS (CATDS), at IFREMER, Plouzané, France. The ECMWF's computing and archive facilities were used to obtain the ERA-Interim wind fields. The manuscript benefited from constructive comments of two anonymous reviewers.

References

Aumont, O., & Bopp, L. (2006). Globalizing results from ocean in situ iron fertilization studies. *Global Biogeochemical Cycles*, *20*, GB2017. https://doi.org/10.1029/2005GB002591

Aumont, O., Ethé, C., Tagliabue, A., Bopp, L., & Gehlen, M. (2015). PISCES-v2: An ocean biogeochemical model for carbon and ecosystem studies. *Geoscientific Model Development*, *8*(8), 2465–2513. https://doi.org/10.5194/gmd-8-2465-2015

Bakker, D. C. E., Pfeil, B., Landa, C. S., Metzl, N., O'Brien, K. M., Olsen, A., et al. (2016). A multi-decade record of high quality fCO2 data in version 3 of the Surface Ocean CO2 Atlas (SOCAT). *Earth System Science Data*, *8*, 383–413. https://doi.org/10.5194/essd-8-383-2016

Blunden, J., Arndt, D. S., & Baringer, M. O. (2011). State of the climate in 2010. *Bulletin of the American Meteorological Society*, *92*(6), S1–S236. https://doi.org/10.1175/1520-0477-92.6.S1

Breeden, M. L., & McKinley, G. A. (2016). Climate impacts on multidecadal pCO_2 variability in the North Atlantic: 1948-2009. *Biogeosciences*, *13*, 3387–3396. https://doi.org/10.5194/bg-13-3387-2016

Brierley, C., & Wainer, I. (2017). Interannual variability in the tropical Atlantic from the last glacial maximum into future climate projections simulated by CMIP5/PMIP3. *Climate of the Past Discussions*, *2017*, 1–34. https://doi.org/10.5194/cp-2017-145

Chen, S.-F., & Wu, R. (2017). An enhanced influence of sea surface temperature in the tropical northern Atlantic on the following winter ENSO since the early 1980s. *Atmospheric and Oceanic Science Letters*, *10*(2), 175–182. https://doi.org/10.1080/16742834.2016.1259542

Conkright, M. E., Locarnini, R. A., Garcia, H. E., O'Brien, T. D., Boyer, T. P., Stephens, C., & Antonov, J. I. (2002). *World ocean atlas2001: Objective analyses, data statistics, and figures, CD-ROM Documentation*. SilverSpring, MD: National Oceanographic Data Center.

Dai, A., & Trenberth, K. E. (2002). Estimates of freshwater discharge from continents: Latitudinal and seasonal variations. *Journal of Hydrometeorology*, *3*, 660–687. https://doi.org/10.1175/1525-7541(2002)003<0660:EOFDFC>2.0.CO;2

Dee, D. P., Uppala, S. M., Simmons, A. J., Berrisford, P., Poli, P., Kobayashi, S., et al. (2011). The ERA-interim reanalysis: Configuration and performance of the data assimilation system. *Quarterly Journal of the Royal Meteorological Society*, *137*(656), 553–597. https://doi.org/10.1002/qj.828

Deser, C., Phillips, A. S., & Alexander, M. A. (2010). Twentieth century tropical sea surface temperature trends revisited. *Geophysical Research Letters*, *37*, L10701. https://doi.org/10.1029/2010GL043321

Dickson, A. G., & Millero, F. J. (1987). A comparison of the equilibrium constants for the dissociation of carbonic acid in seawater media. *Deep Sea Research*, *34*(10), 1733–1743. https://doi.org/10.1016/0198-0149(87)90021-5

Enfield, D. B., Mestas, A. M., Mayer, D. A., & Cid-Serrano, L. (1999). How ubiquitous is the dipole relationship in tropical Atlantic sea surface temperatures? *Journal of Geophysical Research*, *104*, 7841–7848. https://doi.org/10.1029/1998JC900109

Enfield, D. B., Mestas-Nuñez, A. M., & Trimble, P. J. (2001). The Atlantic multidecadal oscillation and its relation to rainfall and river flows in the continental US. *Geophysical Research Letters*, *28*(10), 2077–2080. https://doi.org/10.1029/2000GL012745

Feely, R. A., Wanninkhof, R., Cosca, C. E., Murphy, P., Lamb, M. F., & Steckley, M. D. (1995). CO_2 distributions in the equatorial Pacific during the 1991–1992 ENSO event. *Deep-Sea Research Part II: Topical Studies in Oceanography*, *42*(2–3), 365–386. https://doi.org/10.1016/0967-0645(95)00027-N

Foltz, G. R., & McPhaden, M. J. (2006). Unusually warm sea surface temperatures in the tropical North Atlantic during 2005. *Geophysical Research Letters*, *33*, L19703. https://doi.org/10.1029/2006GL027394

Fratantoni, D. M., & Glickson, D. A. (2001). North Brazil Current ring generation and evolution observed with SeaWiFS. *Journal of Physical Oceanography*, *32*, 1058–1074.

Hong, C.-C., Lee, M.-Y., Hsu, H.-H., Lin, N.-H., & Tsuang, B.-J. (2015). Tropical SST forcing on the anomalous WNP subtropical high during July–August 2010 and the record-high SST in the tropical Atlantic. *Climate Dynamics*, *45*(3-4), 633–650. https://doi.org/10.1007/s00382-014-2275-5

Ibánhez, J. S. P., Araujo, M., & Lefèvre, N. (2016). The overlooked tropical oceanic CO_2 sink. *Geophysical Research Letters*, *43*, 3804–3812. https://doi.org/10.1002/2016GL068020

Ibánhez, J. S. P., Diverres, D.Araujo, M. & Lefevre, N. (2015). Seasonal and interannual variability of sea-air CO2 fluxes in the tropical Atlantic affected by the Amazon River plume. *Global Biogeochemical Cycles*, *29*, 1640–1655. https://doi.org/10.1002/2015GB005110

Ibánhez, J. S. P., Flores, M., & Lefèvre, N. (2017). Collapse of the tropical and subtropical North Atlantic CO_2 sink in boreal spring of 2010. *Scientific Reports*, *7*(1), –9. https://doi.org/10.1038/srep41694

Key, R. M., Kozyr, A., Sabine, C., Lee, K., Wanninkhof, R., Bullister, J. L., et al. (2005). A global ocean carbon climatology: Results from GLODAP. *Global Biogeochemical Cycles*, *19*, GB4031. https://doi.org/10.1029/2004GB002247

Le Quéré, C., Orr, J. C., Monfray, P., Aumont, O., & Madec, G. (2000). Interannual variability of the oceanic sink of CO_2 from 1979 through 1997. *Global Biogeochemical Cycles*, *14*(4), 1247–1265. https://doi.org/10.1029/1999GB900049

Lefèvre, N., Caniaux, G., Janicot, S., & Gueye, A. K. (2013). Increased CO_2 outgassing in February–May 2010 in the tropical Atlantic following the 2009 Pacific El Niño. *Journal of Geophysical Research: Atmospheres*, *118*, 1645–1657. https://doi.org/10.1002/jgrc.20107

Lefèvre, N., Urbano, D. F., Gallois, F., & Diverrès, D. (2014). Impact of physical processes on the seasonal distribution of CO_2 in the western tropical Atlantic. *Journal of Geophysical Research: Oceans*, *119*, 646–663. https://doi.org/10.1002/2013JC009248

Levine, N. M., Doney, S. C., Lima, I., Wanninkhof, R., Bates, N. R., & Feely, R. A. (2011). The impact of the North Atlantic Oscillation on the uptake and accumulation of anthropogenic CO_2 by North Atlantic Ocean mode waters. *Global Biogeochemical Cycles*, *25*, GB3022. https://doi.org/10.1029/2010GB003892

Loptien, U., & Eden, C. (2010). Multidecadal CO2 uptake variability of the North Atlantic. *Journal of Geophysical Research (Atmospheres)*, *115*, D12113. https://doi.org/10.1029/2009JD012431

Ludwig, W., Probst, J.-L., & Kempe, S. (1996). Predicting the oceanic input of organic carbon by continental erosion. *Global Biogeochemical Cycles*, *10*(1), 23–41. https://doi.org/10.1029/95GB02925

Mayorga, E., Seitzinger, S. P., Harrison, J. A., Dumont, E., Beusen, A. H. W., Bouwman, A. F., et al. (2010). Global nutrient export from WaterSheds 2 (NEWS 2): Model development and implementation. *Environmental Modelling & Software*, *25*, 837–853. https://doi.org/10.1016/j.envsoft.2010.01.007

Mehrbach, C., Culberson, C. H., Hawley, J. E., & Pytkowicz, R. M. (1973). Measurement of the apparent dissociation constants of carbonic acid in seawater at atmospheric pressure. *Limnology and Oceanography*, *18*, 897–907. https://doi.org/10.4319/lo.1973.18.6.0897

Menna, M., Faye, S., Poulain, J.-M., Centurioni, L., Lazar, A., Gaye, A., et al. (2016). Upwelling features off the coast of North-Western Africa in 2009–2013. *Bollettino di Geofisica Teorica ed Applicata*, *57*(1), 71–86. https://doi.org/10.4430/bgta0164

Park, G.-H., & Wanninkhof, R. (2012). A large increase of the CO_2 sink in the western tropical North Atlantic from 2002 to 2009. *Journal of Geophysical Research*, *117*, C08029. https://doi.org/10.1029/2011JC007803

Park, G.-H., Wanninkhof, R., Doney, S. C., Takahashi, T., Lee, K., Feely, R. A., et al. (2010). Variability of global net sea-air CO_2 fluxes over the last three decades using empirical relationships. *Tellus Series B: Chemical and Physical Meteorology*, *62B*, 352–368.

Pierrot, D., Neill, C., Sullivan, K., Castle, R., Wanninkhof, R., Lüger, H., et al. (2009). Recommendations for autonomous underway pCO_2 measuring systems and data-reduction routines. *Deep Sea Research*, *56*, 512–522. https://doi.org/10.1016/j.dsr2.2008.12.005

Reynolds, R. W., Smith, T. M., Liu, C., Chelton, D. B., Casey, K. S., & Schlax, M. G. (2007). Daily high resolution blended analysis for sea surface temperature. *Journal of Climate*, *20*, 5473–5496. https://doi.org/10.1175/2007JCLI1824.1

Roy, T., Bopp, L., Gehlen, M., Schneider, B., Cadule, P., Frölicher, T. L., et al. (2011). Regional impacts of climate change and atmospheric CO_2 on future ocean carbon uptake: A multimodel linear feedback analysis. *Journal of Climate*, *24*(9), 2300–2318. https://doi.org/10.1175/2010JCLI3787.1

Rugg, A., Foltz, G. R., & Perez, R. C. (2016). Role of mixed layer dynamics in tropical North Atlantic interannual sea surface temperature variability. *Journal of Climate*, *29*(22), 8083–8101. https://doi.org/10.1175/JCLI-D-15-0867.1

Schuster, U., McKinley, G. A., Bates, N., Chevallier, F., Doney, S. C., Fay, A. R., et al. (2013). An assessment of the Atlantic and Arctic sea–air CO2 fluxes, 1990–2009. *Biogeosciences*, *10*, 607–627. https://doi.org/10.5194/bg-10-607-2013

Sweeney, C., Gloor, E., Jacobson, A. R., Key, R. M., McKinley, G., Sarmiento, J. L., & Wanninkhof, R. (2007). Constraining global air-sea gas exchange for CO_2 with recent bomb ^{14}C measurements. *Global Biogeochemical Cycles*, *21*, GB2015. https://doi.org/10.1029/2006GB002784

Takahashi, T., Olafsson, J., Goddard, J. G., & Chipman, D. W. (1993). Seasonal variation of CO_2 and nutrients in the high-latitude surface oceans: A comparative study. *Global Biogeochemical Cycles*, *7*(4), 843–878. https://doi.org/10.1029/93GB02263

Takahashi, T.,Sutherland, S. C.,Chipman, D.W.,Goddard, J. G., Ho, C.,Newsberger, T., et al. (2014). Climatological distributions of pH, pCO_2,total CO_2, alkalinity and $CaCO_3$ saturation in the global surface ocean, and temporal changes at selectedlocations. *Marine Chemistry*, *164*, 95–125. https://doi.org/10.1016/j.marchem.2014.06.004

Taschetto, A., Rodrigues, R., Meehl, G., McGregor, S., & England, M. (2016). How sensitive are the Pacific–tropical North Atlantic teleconnections to the position and intensity of El Niño-related warming? *Climate Dynamics*, *46*(5–6), 1841–1860. https://doi.org/10.1007/s00382-015-2679-x

Taylor, K. E. (2001). Summarizing multiple aspects of model performance in a single diagram. *Journal of Geophysical Research*, *106*, 7183–7192. https://doi.org/10.1029/2000JD900719

Valsala, V. K., Roxy, M. K., Ashok, K., & Murtugudde, R. (2014). Spatiotemporal characteristics of seasonal to multidecadal variability of pCO_2 and air-sea CO_2 fluxes in the equatorial Pacific Ocean. *Journal of Geophysical Research: Oceans*, *119*, 8987–9012. https://doi.org/10.1002/2014JC010212

Weiss, R. F. (1974). CO_2 in water and seawater: The solubility of a non-ideal gas. *Marine Chemistry*, *2*, 203–215. https://doi.org/10.1016/0304-4203(74)90015-2